Molecular architecture of the human sinus node

- insights into the function of the cardiac pacemaker

Short title: Molecular architecture of the human sinus node

Natalie J. Chandler, BSc[1]; Ian D. Greener, PhD[1]; James O. Tellez, PhD[1]; Shin Inada, PhD[1]; Hanny Musa, PhD[1]; Peter Molenaar, PhD[2]; Dario DiFrancesco, MD[3]; Mirko Baruscotti, PhD[3]; Renato Longhi, PhD[3]; Robert H. Anderson, MD[1];Rudolf Billeter, PhD[4]; Vinod Sharma, MD[5], Daniel C. Sigg, MD[5]; Mark R. Boyett, PhD[1] and Halina Dobrzynski, PhD[1]

[1]University of Manchester, UK

[2]Queensland University of Technology & University of Queensland, Australia

[3]University of Milano, Italy

[4]University of Nottingham, UK;

[5]Medtronic Inc., USA

Correspondence to Dr. H. Dobrzynski, Cardiovascular Research Group,

Faculty of Medical and Human Sciences, University of Manchester, Core Technology Facility,

46 Grafton Street, Manchester M13 9NT, UK. E-mail: halina.dobrzynski@manchester.ac.uk

Word count: 7397

Abstract

Background-Although we know much about the molecular make-up of the sinus node (SN) in small mammals, little is known about it in the human. The aims of this study were to investigate the expression of ion channels in the human SN and to use the data to predict electrical activity.

Methods and Results-Quantitative PCR, *in situ* hybridisation and immunofluorescence were used to analyse six human tissue samples. mRNA for 120 ion channels (and some related proteins) were measured in the SN, a novel 'paranodal area' (PN) and the right atrium (RA). The results show for example that in the SN, as compared to the RA, there is a lower expression of $Na_v1.5$, $K_v4.3$, $K_v1.5$, ERG, $K_{ir}2.1$, $K_{ir}6.2$, RyR2, SERCA2a, Cx40 and Cx43 mRNAs, but a higher expression of $Ca_v1.3$, $Ca_v3.1$, HCN1 and HCN4 mRNAs. The expression pattern of many ion channels in the PN was intermediate between that of the SN and RA. However, the PN showed greater expression in comparison to the SN and RA of $K_v4.2$, $K_{ir}6.1$, TASK1, SK2 and MiRP2. Expression of ion channel proteins was in agreement with the expression of the corresponding mRNAs. The levels of mRNA in the SN, as a percentage of those in the RA, were used to estimate conductances of key ionic currents as a percentage of those in a mathematical model of the human atrial action potential. The resulting SN model successfully produced pacemaking.

Conclusions-Ion channels show a complex and heterogeneous pattern of expression in the SN, PN and RA in the human and the expression pattern is appropriate to explain pacemaking.

Key Words: sinus node; pacemaker; ion channels

Introduction

The sinus node (SN), the primary cardiac pacemaker, is complex and heterogeneous.[1] The action potential originates in the SN and then propagates into the surrounding muscle of the right atrium (RA).[1] The SN is highly adapted to its role as the primary pacemaker - while its mix of ionic currents fits it for pacemaking, its poor electrical coupling protects it from the inhibitory hyperpolarizing influence of the surrounding RA.[1,2] Since its discovery by Keith and Flack in 1907,[3] a wealth of data has been accrued on this specialised tissue in small mammals, particularly concerning the action potential and the underlying ionic currents. However, only one action potential has been published from the adult human SN,[4] and this came from a diseased heart subjected to a range of treatments. Consequently, there is little information available on the nature of the action potential in the human SN and the ionic currents underlying it. The molecular basis of the ionic currents involved in the SN action potential has recently been established for both the

rabbit[5] and mouse.[6] However, the 'molecular architecture' of the human SN has not been elucidated. Of particular interest are ion channels and Ca^{2+}-handling proteins that are key to the electrical activity.[1,2] Mutations in ion channels in humans ($Na_v1.5$, HCN4) as well as the knockout of ion channels ($Ca_v1.3$, $Ca_v3.1$) in mice have been linked with sick sinus syndrome or bradycardia.[7] The primary aim of this study was to investigate ion channels, along with Ca^{2+}-handling proteins, connexins, receptors and cell type-markers, at the mRNA and protein levels in the SN and the surrounding RA in the human. Our data reveal a complex expression of ion channels, and demonstrate a previously undescribed *paranodal area* (PN) within the terminal crest. The secondary aim was to use a functional genomics approach, integrating the expression of ion channels using mathematical modelling, to predict the electrical activity in the SN. Using a new method of building cell membrane models, in which mRNA levels are used to estimate ionic conductances, we were able to demonstrate the potential for spontaneous electrical activity within the SN.

Methods

We obtained six specimens of the area of RA containing the SN and PN from non-failing healthy hearts from the Prince Charles Hospital District, Chermside, Australia (ethics approval, EC2565; work was also ethically approved by University of Manchester). A clinical profile of the donors is shown in the Online Data Supplement (ODS; Table S1). We used quantitative PCR (qPCR), *in situ* hybridization (ISH), histology, immunofluorescence and mathematical modelling to investigate the molecular make-up (and predict function) of the human SN, PN and RA. Detailed descriptions of the methods are given in the ODS.

Sampling of sinus node, paranodal area and atrial muscle for qPCR

We sampled SN, PN and RA (outlined in red, green, and yellow in Figure 1A) from 50-100 histological sections from the head, body and tail of the SN (as defined by Sanchez Quintana *et al.*[8]). Following extraction of RNA, the amounts of ~120 mRNAs for cell type-markers, ion channels, Ca^{2+}-handling proteins, connexins and receptors were measured using qPCR. Here, we describe only the mRNAs for major ion channels or mRNAs that vary among tissues. All data are shown in the ODS (Figures S1-S6).

Statistical analysis

Means ± SEM are shown. Significant differences in the abundance of mRNAs and proteins in different tissues were identified using one-way ANOVA and paired t-tests. A difference was assumed to be significant when $P<0.05$. In some figures, absolute P values are shown. For cluster analysis, ΔCT values for each mRNA were transformed to $\log_{10}$ and centred. This resulted in a distribution for each mRNA with a

mean of 0 and a standard deviation of 1. Because not all the resulting data were normally distributed, SAM (statistical analysis of microarrays, a bootstrap method, which is tolerant to non-normality) was used to test differences in mRNA abundance between SN and PN, SN and RA, and PN and RA. A more detailed description of the statistical analysis used in this study can be found in the ODS.

Statement of Responsibility

The authors had full access to and take full responsibility for the integrity of the data. All authors have read and agree to the manuscript as written.

Results

Morphological characteristics of sinus node, paranodal area and atrial muscle

Sectioning the terminal crest revealed the location of the SN upon staining with Masson's trichrome (Figure 1A). The SN was clearly identifiable on the basis of the presence of the SN artery and the large amount of connective tissue (stained blue; myocytes stained purple/pink). Interestingly, sections through the SN also showed a discrete area, composed of loosely packed myocytes, which we have termed the *paranodal area* (PN). The PN is close to but not continuous with the SN as shown in Figure 1A. Immunofluorescence showed that this area consisted of a mixture of myocytes expressing and lacking two marker proteins: connexin43 (Cx43), responsible for electrical coupling, and atrial natriuretic peptide (ANP), a hormone secreted by atrial muscle (Figure 1B,C; white and blue arrows highlight myocytes expressing or lacking, respectively, markers). Both Cx43 and ANP are known to be absent from the SN but abundantly expressed in the RA in small mammals.[5,6] Our immunofluorescence analysis revealed this also to be the case in the human (Figure 1B,C).

House keeping genes and nodal markers

For qPCR, the level of each transcript is given relative to a housekeeping gene to correct for variations in input RNA. mRNA levels of two housekeeper genes were measured: 28S and GAPDH. The level of both was similar in each of the three tissues. We chose 28S for our analysis, although similar results were obtained using GAPDH. ANP and Tbx3 (transcription factor known to be expressed in SN of small mammals[9]) were used to characterise the tissues studied by qPCR. qPCR showed ANP to be highly abundant in the PN and RA, but poorly expressed in the SN (Figure 2A). This was confirmed by ISH (Figure 3A,B) – note the mixture of ANP expressing (e.g. green arrows) and non-expressing (e.g. red arrows) myocytes in the PN (Figure 3B). qPCR showed Tbx3 to be abundant in the SN, but poorly expressed in the RA; there was an

intermediate level of expression in the PN (Figure 2B). The poor expression of ANP, but high expression of Tbx3, in the SN demonstrated by qPCR confirms that during dissection the SN tissue was not contaminated with RA tissue.

Na^+ channels

Voltage-gated Na^+ channels are responsible for the inward Na^+ current, I_{Na}. I_{Na} is responsible for the rapid action potential upstroke seen in the working myocardium. Studies in small mammals show that there is little or no measurable I_{Na} in the centre of the SN.[1,2] qPCR showed that mRNA for the cardiac Na^+ channel, $Na_v1.5$, was SN<PN<RA (Figure 2E). This was confirmed by ISH (Figure 3C) and immunohistochemistry showed that $Na_v1.5$ protein was expressed in a similar manner (Figure 4).

Recently, in small mammals, other Na^+ channels have also been shown to be expressed in cardiac myocytes and have a role in the SN action potential.[10] There was a complex expression of other Na^+ channels in the three regions (Figure 2C,D; ODS-Figure S2). At the mRNA level, their expression levels were >100-fold lower than $Na_v1.5$, suggesting that these Na^+ channels may not play a significant role in the human. Of the Na^+ channel β-subunits ($Na_v\beta1$-$Na_v\beta4$), $Na_v\beta1$ was the most abundant β-subunit at the mRNA level, and its expression was SN<PN<RA (Figure 2F; ODS-Figure S2).

Ca^{2+} channels

Two separate Ca^{2+} currents have been recorded from SN cells, the long-lasting type ($I_{Ca,L}$) and the transient type (I_{CaT}).[1,2,7] I_{CaL} has been shown to have a role in the upstroke of the SN action potential and may have a role in diastolic depolarization.[1,2,7] I_{CaT} has been shown to have a role in diastolic depolarization.[1,2,7] The ion channels responsible for I_{CaL} are $Ca_v1.2$ and $Ca_v1.3$ and for I_{CaT}, $Ca_v3.1$-$Ca_v3.3$. $Ca_v1.2$ mRNA was ~10-fold more abundant than $Ca_v1.3$ mRNA (Figure 2G,H). As measured using qPCR, the $Ca_v1.2$ mRNA level tended to be SN<PN=RA, but this difference was not significant (Figure 2G). At the protein level, as determined by immunofluorescence, the amount of $Ca_v1.2$ was SN<PN=RA (ODS-Figure S7). Both qPCR (Figure 2H) and ISH (Figure 3D) showed the level of $Ca_v1.3$ mRNA to be SN>PN=RA. $Ca_v3.1$ mRNA was at least 10-fold more abundant than $Ca_v3.2$ and $Ca_v3.3$ mRNAs; $Ca_v3.2$ mRNA was below the detection threshold (ODS-Figure S2). Like $Ca_v1.3$ mRNA, $Ca_v3.1$ mRNA (Figure 2I) and protein (ODS-Figure S7) were SN>PN=RA; $Ca_v3.3$ mRNA tended to show a similar pattern (ODS-Figure S2). Perhaps like $Ca_v1.2$ mRNA, mRNAs for the Ca^{2+} channel subunits, $Ca_v\alpha2\delta3$ and $Ca_v\gamma4$, were SN<PN=RA (ODS-Figure S2).

mRNAs for other Ca^{2+} channel subunits ($Ca_v\beta1$-$Ca_v\beta3$, $Ca_v\alpha2\delta1$ and $Ca_v\alpha2\delta2$) did not vary among the three regions (ODS-Figure S2).

HCN channels

The HCN channels are responsible for the hyperpolarization-activated or 'funny' current, I_f.[1,2,7] This has a key role in the pacemaker potential of the SN.[2] There are four members in the HCN family, HCN1-HCN4. The levels of both HCN1 and HCN4 mRNAs were SN>PN=RA (Figure 2J,L). The level of HCN2 mRNA, in contrast, was SN<PN<RA (Figure 2K). HCN3 mRNA expression was negligible in all tissues (ODS-Figure S2). HCN4 mRNA was more abundant than mRNA for the other isoforms and it was investigated at the protein level using immunofluorescence. Figure 5 shows HCN4 protein to be expressed in the sarcolemma of the SN myocytes, but was below the detection threshold with the immunohistochemical method in both the PN and RA.

Transient outward K^+ channels

The transient outward K^+ current (I_{to}) is responsible for the early phase of repolarization (phase 1) of the action potential. The ion channels responsible for I_{to} are the voltage-dependent K^+ channels, $K_v1.4$, $K_v4.2$ and $K_v4.3$. $K_v4.3$ is regarded as the major ion channel underlying I_{to} in the human and $K_v4.3$ mRNA was at least 10-fold more abundant than $K_v1.4$ and $K_v4.2$ mRNAs (Figure 6A-C). The pattern of expression of $K_v4.3$ mRNA (Figure 6C) and protein (ODS-Figure S8) was SN=PN<RA. Interestingly, $K_v1.4$ mRNA was SN=RA>PN, whereas $K_v4.2$ mRNA was SN=PN>RA (Figure 6A,B).

Delayed rectifier K^+ channels

There are three delayed rectifier K^+ currents, ultra-rapid (I_{Kur}), rapid (I_{Kr}) and slow (I_{Ks}). The ion channels responsible for I_{Kur}, I_{Kr} and I_{Ks} are $K_v1.5$, ERG and K_vLQT1, respectively. At the mRNA level, the amounts of the three ion channels were comparable (Figure 6D-F). Both $K_v1.5$ and ERG mRNAs were SN<PN=RA and K_vLQT1 mRNA tended to be distributed in a similar manner (Figure 6D-F). Immunofluorescence showed $K_v1.5$ protein to be distributed in the same manner as its mRNA (ODS-Figure S8).

Inward rectifier K^+ channels

The background inward rectifier K^+ current, I_{K1}, is generated by the ion channels, $K_{ir}2.1$-$K_{ir}2.4$. $K_{ir}2.1$ and $K_{ir}2.3$ mRNAs were ~10-fold more abundant than $K_{ir}2.2$ and $K_{ir}2.4$ mRNAs (ODS-Figure S4). $K_{ir}2.1$ mRNA level was SN=PN<RA (Figure 6G). $K_{ir}2.3$ mRNA also tended to be less in the SN (Figure

6H). We have also previously shown that, in the human, $K_{ir}2.1$ protein is expressed in the RA, but not in the SN.[7] The acetylcholine (ACh) activated K^+ current, I_{KACh}, is generated by a heteromultimer of $K_{ir}3.1$ and $K_{ir}3.4$.[11] $K_{ir}3.1$ mRNA was ~10-fold more abundant than $K_{ir}2.1$ and $K_{ir}2.3$ mRNAs; neither $K_{ir}3.1$ mRNA and protein nor $K_{ir}3.4$ mRNA varied among tissues (ODS-Figures S4 and S8). In the heart, the ATP-sensitive K^+ current, I_{KATP}, is thought to be generated by the α-subunit, $K_{ir}6.2$, and the β-subunit, SUR2A. Surprisingly, the abundance of $K_{ir}6.1$ mRNA was similar to that of $K_{ir}6.2$ mRNA (ODS-Figure S4). $K_{ir}6.2$ mRNA was SN<PN=RA (ODS-Figure S4), but interestingly, $K_{ir}6.1$ mRNA was SN=RA<PN (Figure 6I). SUR2A mRNA did not vary among the tissues (ODS-Figure S4).

Other K^+ channels

mRNAs for $K_v1.2$, $K_v1.6$, $K_v1.7$ and $K_v2.1$ were generally weakly expressed in the three tissues (ODS-Figure S3). Nevertheless, $K_v1.2$ mRNA was significantly less in the PN than in the RA, whereas $K_v1.6$ and $K_v1.7$ mRNAs were SN<PN=RA (ODS-Figure S3). TASK1 and TWIK1 are twin-pore domain K^+ channels that are expressed in cardiac muscle, albeit their function is unclear. mRNAs for both channels were highly abundant – comparable to $K_v1.5$, K_vLQT1 and $K_{ir}2.1$ mRNAs for example (ODS-Figure S4). TASK1 mRNA was SN=RA<PN (Figure 6J), whilst TWIK1 mRNA was SN<PN=RA (ODS-Figure S4). There are three small conductance Ca^{2+}-activated K^+ channels, SK1-SK3. SK channels are responsible for Ca^{2+}-activated K^+ current, I_{KCa}, and play a role in the repolarization of the human atrial action potential;[12] SK2 has been shown to be coupled to $Ca_v1.2$ and $Ca_v1.3$ via α-actinin2.[13] SK2 and SK3 mRNAs were abundant (abundance comparable to that of $K_{ir}2.1$ mRNA for example); SK1 mRNA was ~10-fold less abundant (ODS-Figure S4). SK2 mRNA was SN=RA<PN (Figure 6K).

We also studied accessory proteins for K^+ channels. Three β-subunits are thought to regulate the delayed rectifier K^+ channels, $K_v\beta1$-$K_v\beta3$. $K_v\beta2$ mRNA tended to be the most abundant; $K_v\beta2$ mRNA was SN<PN (ODS-Figure S4). MiRPs are suggested to regulate delayed rectifier K^+, transient outward K^+ and HCN channels.[14] At the mRNA level, MiRP2 and MiRP3 were more abundant than MiRP1 (ODS-Figure S4); MiRP2 mRNA was SN=RA<PN (Figure 6L). Of accessory proteins thought to regulate transient outward K^+ channels, at the mRNA level, frequenin (a Ca^{2+}-binding protein known to regulate K_v4 channels)[15] was SN>PN=RA, KChIP2 was SN=PN<RA, while DPP6 (dipeptidyl aminopeptidase-like protein 6) and KChAP did not vary among tissues (ODS-Figure S3).

Ca^{2+}-handling proteins

Intracellular Ca^{2+} has been suggested to play an important role in pacemaking in small mammals.[16] The Na^+-Ca^{2+} exchanger, NCX1, at the mRNA (Figure 7A) and protein levels (ODS-Figure S9) did not vary among tissues. RyR2 mRNA (Figure 7B) and protein (ODS-Figure S9) were SN<PN=RA, whereas RyR3 mRNA was SN=PN>RA (Figure 7C). However, RyR2 mRNA was ~1000-fold more abundant than RyR3 mRNA (Figure 7B,C). The sarcoplasmic reticulum (SR) Ca^{2+} pump, SERCA2a, both at the mRNA (Figure 7D) and protein (ODS-Figure S9) levels, was SN<PN=RA. Phospholamban and sarcolipin regulate SERCA2a and, at the mRNA level, they were of comparable abundance; sarcolipin was SN<PN=RA and phospholamban had a similar distribution (ODS-Figure S5). PMCA1 and PMCA4 are plasmalemmal Ca^{2+} ATPases; PMCA4 mRNA was ~10-fold more abundant than PMCA1 mRNA (ODS-Figure S5). PMCA1 mRNA was SN=RA<PN, whereas PMCA4 mRNA was SN>PN=RA (ODS-Figure S5). At the mRNA level, all three IP_3 receptors (isoforms 1-3) were detected; isoforms 2 and 3 tended to be most abundantly expressed in the PN (ODS-Figure S5). CaM kinase IIb and FKBP12 were detected, but did not vary among tissues (ODS-Figure S5). TRPC channels have been suggested to be store-operated Ca^{2+} channels and be involved in pacemaking in the SN;[17] five isoforms were detected at the mRNA level (ODS-Figure S5). TRPC6 mRNA was SN>PN>RA (ODS-Figure S5).

Na/K pump

The α1, α2 and α3 isoforms of the Na^+/K^+ pump were detected at the mRNA level; all three isoforms tended to be SN<PN=RA (ODS-Figure S5).

Connexins and cell adhesion proteins

Connexins are responsible for electrical coupling in the heart. At the mRNA level, the levels of Cx40, Cx43 and Cx45 (responsible for 200, 60-100 and 30-40 pS gap junction channels, respectively) were comparable and at least 10-fold greater than that of Cx31.9 (responsible for 30-40 pS gap junction channels) (Figure 7E-H). Both Cx40 mRNA (Figure 7F) and protein (ODS-Figure S7) and Cx43 mRNA (Figure 7G) were SN<PN=RA. The Cx31.9 mRNA level was SN<PN (Figure 7E). Two cell adhesion proteins were investigated at the mRNA level: cadherin and desmoplakin (ODS-Figure S1). Desmoplakin mRNA was SN<PN=RA (Figure 7I).

Receptors

Adenosine, adrenergic and muscarinic receptors were investigated at the mRNA level. A1a, A2a, A2b and A3 adenosine receptors were detectable; A3 receptor mRNA was SN<PN (ODS-Figure S6). α1a,

α1b, α1d, α2a-α2c, β1 and β2 adrenergic receptors were detectable: the α1a receptor mRNA was, SN=PN>RA, the α2a receptor tended to be SN=RA<PN, and the β1 receptor was SN=PN<RA (ODS-Figure S6). Of the muscarinic receptors, M2 did not vary among tissues, whereas M1 was undetectable (ODS-Figure S6).

Summary and consequences for electrical activity

A two-way hierarchical cluster analysis (Pearson distance) for all transcripts is shown in the ODS (Figure S10). The resultant clusters for the samples show the SN to be distinct from the two other tissues. A subset of 66 transcripts which contained fewer than 2.699 estimated false positive calls in three bootstrap comparisons between SN, PN and RA did cluster the samples into the three tissue groups (Figure 8A). Correspondingly, multidimensional scaling (Euclidian distance) using these 66 "indicator" transcripts could also separate the samples according to tissue (Figure 8B). This suggests that the SN is distinct from both the PN and RA, with the PN being intermediate between the other two. The application of a number of different clustering algorithms (details in ODS) yielded four different groups of transcripts that consistently clustered together. The first were mRNAs that were expressed at higher levels in the SN, specifically, $Ca_v1.3$, $Ca_v3.1$, HCN1, HCN4 and frequenin. The second consisted of mRNAs that were expressed at higher levels in the PN, specifically $K_{ir}6.1$, TASK1, SK2, PMCA1 and the A3 adenosine receptor. The mRNAs of the third group were expressed at higher levels in the RA; they coded for ANP, $Na_v1.1$, $Na_v1.4$, $Na_v1.5$, HCN2, $K_v1.5$, $K_v1.7$, $K_{ir}6.2$, RyR2, sarcolipin, Cx43 and desmoplakin. The mRNAs of the fourth were not differentially expressed between the tissues, but the consistent clustering indicates that they correlated well in the individual samples. They all code for accessory subunits to voltage-gated Ca^{2+} channels: $Ca_v\alpha2\delta1$, $Ca_v\alpha2\delta3$, $Ca_v\beta1$ and $Ca_v\beta2$.

What are the consequences of the unique pattern of expression of ion channels in the human SN on electrical activity in this tissue? It was assumed that whole cell conductance for a particular ionic current is roughly proportional to the abundance of one or more mRNAs responsible for the relevant ion channel, ignoring the possible non-linearity of the relationship between transcript abundance and conductance. For each of the major ionic currents (I_{Na}, I_{CaL}, I_{to}, I_{Kur}, I_{Kr}, I_{Ks} and I_{K1}), the sum of relevant mRNAs in the SN was calculated and expressed as a percentage of the sum of the same mRNAs in the RA (ODS-Table S7). This was assumed to be equal to the conductance of the relevant ionic current in the SN expressed as a percentage of the conductance in the RA. Na^+-Ca^{2+} exchange, SR Ca^{2+} release and SR Ca^{2+} uptake were scaled in an

analogous way (ODS-Table S7). Control values for human RA were taken from the mathematical model of Courtemanche *et al.*[18] for the human atrial action potential (based on extensive electrophysiological data from human RA). The human SN expresses the mRNAs responsible for I_{CaT} and I_f (Figure 2). Because of the absence of these ionic currents in the model (and low expression of corresponding mRNAs in RA; Figure 2), a different approach was adopted for these ionic currents. The conductance for I_{CaT} was assumed to be the same as in rabbit SN cells, and the conductance for I_f was taken from the study of the human SN of Verkerk *et al.*[4] To validate this approach, the mRNA abundance in human ventricular muscle was used to predict electrical activity in human ventricular muscle – the result was the well known form of the human ventricular action potential (data not shown). This approach was then used to predict the electrical activity of the human SN by the modification of nine ionic currents and the three Ca^{2+}-handling proteins (ODS-Table S7). The calculated human atrial action potential from the unmodified Courtemanche *et al.*[18] model and the calculated human SN action potential as predicted from the model are shown in Figure 8C. The upstroke velocity of the action potential and the accompanying intracellular Ca^{2+} transients are also shown. The trace produced is a typical pacemaker action potential with a slow upstroke velocity (Figure 8C). There was little change in the action potential when only one of the 12 ionic currents and Ca^{2+}-handling proteins was altered and the pacemaker action potential was only obtained when all nine ionic currents were altered (ODS-Figures S11 and S12). Figure 8C shows that, when I_f was blocked, pacemaking was slowed, as has been observed in human SN myocytes.[19] The PN action potential was modelled in the same way as the SN action potential: as compared to the RA action potential, the upstroke velocity and amplitude of the action potential were reduced and the membrane tended to be depolarized during diastole (Figure 8C).

Discussion

This is the first study to investigate the complex expression of ion channels in the human SN and its environs. Our study shows three distinct patterns of molecular expression, revealing the existence of a PN in addition to the SN and RA. The expression pattern of the SN is appropriate for pacemaking.

Differences between sinus node and atrial muscle

The cluster analysis in Figure 8A shows that a large number of mRNAs vary between the SN and the RA. These will be discussed in relation to ionic currents.

I_{Na}. As compared to the RA, $Na_v1.5$ mRNA and protein and the mRNA for the β-subunit, $Na_v\beta1$, were less expressed in the SN (Figures 2- 4). In small mammals, whereas in the RA there is a large I_{Na} and $Na_v1.5$

is abundantly expressed, in the SN I_{Na} is small or absent and the expression of $Na_v1.5$ mRNA[5,6] and protein[7,10] is minimal. As a consequence, whereas the upstroke of the RA action potential is fast, the upstroke of the SN action potential is slow (I_{Na} is responsible for upstroke of atrial action potential) (Figure 8C). $Na_v1.5$ and $Na_v\beta1$ knockout mice have SN dysfunction, with bradycardia and increased SN conduction times.[20,21] In humans, mutations in $Na_v1.5$ have been linked to familial sick sinus syndrome.[7] Therefore, despite the lower abundance of $Na_v1.5$ in the SN, it must still have a functional role. Na^+ channels other than $Na_v1.5$ are also known to be important in the function of the mouse SN.[10] However, Na^+ channels other than $Na_v1.5$ were poorly expressed in the human SN (Figure 2) and this suggests that they may not play a large role.

I_{CaL}. As compared to the RA, $Ca_v1.2$ mRNA and protein tended to be less abundant in the SN, whereas $Ca_v1.3$ mRNA was more abundant (Figures 2 and 3; ODS-Figure S7). In small mammals, in the absence of I_{Na}, I_{CaL} is responsible for the slow upstroke of the action potential in the SN.[1] In rabbit, an 'isoform switch' from $Ca_v1.2$ to $Ca_v1.3$ in the SN, similar to that in the human, has been reported.[5] Two studies on $Ca_v1.3$ knockout mice have shown SN dysfunction with bradycardia and spontaneous arrhythmias.[22]

***I_{CaT}* and *I_f*.** $Ca_v3.1$ and HCN4, the major ion channels responsible for I_{CaT} and I_f, at both the mRNA and protein levels, were expressed in greater amounts in the SN than in the RA (Figures 2 and 5; ODS-Figure S7). This is consistent with mRNA data from the mouse[6] and rabbit.[5] In small mammals, I_{CaT} and I_f have been shown to be important in pacemaking in the SN, and their pharmacological block slows pacing rate.[7] In addition, the $Ca_v3.1$ knockout mouse has bradycardia.[23] In the HCN4 knockout mouse, I_f is reduced by 85% in the SN, the heart rate is reduced by 37%, and the embryo dies between embryonic days 9.5 and 11.5.[24] I_f has recently been recorded from human SN myocytes and pharmacological block of I_f slows pacemaking[4] (see also Figure 8C). In humans, mutations in HCN4 have been linked to familial sick sinus syndrome.[7]

***I_{to}*.** The major ion channel responsible for I_{to} in the human, $K_v4.3$, at the mRNA and protein levels, was less abundant in the SN than in the RA (Figure 6; ODS-Figure S8). I_{to} is responsible for the early phase of repolarization (phase 1) and it also helps determine action potential duration.[1] In the rabbit, the density of I_{to} is lower in the SN than in the RA[1] and the corresponding ion channel ($K_v1.4$; there are well known species

differences in ion channels responsible for I_{to}) is less abundant in the SN than in the RA. It is likely that in the human as in the rabbit the density of I_{to} will be less in the SN than in the RA.

I_{Kur}, I_{Kr} and I_{Ks}. As with $K_v4.3$, the ion channels responsible for I_{Kur}, I_{Kr} and I_{Ks} ($K_v1.5$, ERG and K_vLQT1), at the mRNA level (and protein level in case of $K_v1.5$), tended to be less expressed in the SN than in the RA (Figure 6; ODS-Figure S8). It is well known that, in the rabbit, the action potential duration decreases down the conduction pathway from the SN to the RA[1] and it is possible that this is also true in the human as a result of the decrease in expression of e.g. $K_v4.3$, $K_v1.5$ and ERG in the SN.

I_{K1}. $K_{ir}2.1$ and $K_{ir}2.3$, likely to be major ion channels responsible for I_{K1}, tended to be less abundant in the SN than in the RA (Figure 6). This is expected, because in small mammals the presence of I_{K1} in the working myocardium is known to be responsible for its stable resting potential, whereas in the SN I_{K1} is small or absent and as a result there is no stable resting potential and instead there is pacemaking.[7] The knockdown of $K_{ir}2.1$ by ~80% in the ventricles has been used as a potential strategy for the creation of a biopacemaker.[25]

I_{KACh}. The two ion channels responsible for I_{KACh}, $K_{ir}3.1$ and $K_{ir}3.4$, at the mRNA and protein ($K_{ir}3.1$ only) levels, were abundant and did not vary among tissues (ODS-Figures S4 and S8). This is consistent with mRNA and protein data from small mammals.[5,6,26] I_{KACh} is activated on binding of ACh, released from vagal nerves, to M2 receptors; M2 receptors were abundantly expressed in the human SN (ODS-Figure S6).

Ca^{2+}-handling proteins. At the mRNA level and in some cases at the protein level, various Ca^{2+}-handling proteins (RyR2, SERCA2a, sarcolipin) were less abundant in the SN than in the RA (Figure 7; ODS-Figures S5 and S9). Intracellular Ca^{2+} has been suggested to play an important role in pacemaker activity.[16] It has been suggested that some SR Ca^{2+} release occurs during the pacemaker potential. This occurs either in response to I_{CaT} or spontaneously.[16] The diastolic Ca^{2+} release activates the Na^{+}-Ca^{2+} exchanger. Because the exchanger is electrogenic, an inward current is produced (I_{NaCa}), which contributes to the pacemaker potential. In the rabbit, as in the human, RyR2 mRNA is less abundant in the SN than in the RA.[5] Previously, RyR3 mRNA has been shown to be primarily expressed in the cardiac conduction system in mouse[6] and rabbit.[5] Although a similar tendency was observed in the human, RyR3 mRNA was poorly expressed in comparison to RyR2 mRNA (Figure 7).

Connexins. mRNA and protein for the two most abundant connexins (Cx40 and Cx43) was less abundant in the SN than in the RA (Figures 1 and 7; ODS-Figure S7). In small mammals, electrical coupling

is strong in the RA to allow rapid propagation of the action potential, but weak in the SN to protect the SN from the hyperpolarizing influence of the neighbouring RA.[1] Consistent with this and with the observations from the human, in small mammals the expression of Cx40 and Cx43 at the mRNA and protein levels is also reduced in the SN as compared to the RA.[1] In the SN, electrical coupling is presumably provided by Cx45 – in the human, as in small mammals, Cx45 mRNA was abundant in the SN (Figure 7). A mouse deficient in Cx40 shows an increase in SN recovery time and a bradycardia,[27] suggesting that, at least in the mouse, Cx40 is important in SN function.

Gaborit *et al.*[28] have measured the abundance of mRNA for ion channels in various regions of the non-diseased human heart, including the RA; expression levels in the RA are qualitatively similar to those reported here for the RA.

Paranodal area

This study suggests that this area is unique, being similar in some respects to the RA, but in other respects to the SN. As shown in most figures, the PN showed an intermediate pattern of expression of many ion channels similar to that seen in the periphery of the rabbit SN.[5] Results from ISH and immunofluorescence suggest that this is due to a mixture of nodal and atrial cells within the PN (e.g. Figures 1 and 3), again consistent with results from the periphery of the rabbit SN.[5] The PN, however, shows a unique pattern of expression of K^+ channels and accessory subunits. For example, it shows greater expression in comparison to both the SN and RA of $K_v4.2$, $K_{ir}6.1$, TASK1, SK2 and MiRP2 (Figure 6). Expression of $K_{ir}2.1$ mRNA was low in the PN as compared to the RA (Figure 6). It is possible, therefore, that the PN is depolarized as compared to the RA. This may be important – it may electrotonically depolarize the thin layer of RA lying between the PN and SN (Figure 1A) and in this way facilitate the conduction of the action potential from the SN into the RA. In addition, as a result of a low abundance of $K_{ir}2.1$, the PN may be unstable and prone to ectopic activity and it could be responsible for the 'cristal tachycardias' known to originate from this region.[29] The dynamics of atrial fibrillation (AF) are thought to be affected by the expression levels of $K_{ir}2$ channels[30] and, therefore, the PN may play a special role in AF. The leading pacemaker site in the SN is not static and alters in response to external factors such sympathetic and parasympathetic stimulation.[1] This is known as 'pacemaker shift'; perhaps the PN has a role in the shift. Intracellular recordings from the PN are required to determine the function of this novel region.

Conclusions and implications

We have characterised the expression of ion channels in the human SN and its environs, including an extensive novel area, the PN. Our results provide insights into the electrical properties of these cardiac tissues as well as sick sinus syndrome, be it familial, age-related or heart failure-related. For example, mutations in $Na_v1.5$ and HCN4 have been shown to cause familial sick sinus syndrome and our study shows how these ion channels are normally distributed in the human SN.[7] Perhaps the $Na_v1.5$-related dysfunction is the result of loss of I_{Na} from the PN (as it is absent in SN). For treatment of sick sinus syndrome there has been much interest in the creation of a 'biopacemaker'. Recent strategies have included knocking out $K_{ir}2.1$[25] or over-expressing HCN[31] in ventricular myocardium. Our results show that there are many changes in gene expression between the human SN and the RA and this suggests that, for a successful 'biopacemaker' to be developed, the manipulation of more than one gene may be required. In addition, if we understand gene expression, why create a *de novo* pacemaker in an alien environment – why not repair the sick sinus using gene therapy of the ion channels?

Why is the heart rate in the human is ~70 beats/min, whereas in the mouse it is ~400-800 beats/min? Marionneau *et al.*[6] studied ion channel expression at the mRNA level in the mouse SN. Comparison of the two data sets (using mRNA level of $Na_v1.5$ in RA as reference), suggests that whereas the expression of some key ion channels in the SN in the two species is comparable ($Ca_v1.2$, $Ca_v1.3$ and ERG), many key ion channels (and associated accessory subunits) responsible for inward ($Na_v1.5$, $Na_v\beta1$, $Na_v1.4$, $Ca_v3.1$, $Ca_v3.2$ and HCN4) and outward ($K_v1.5$, $K_v2.1$, $K_v4.2$, K_vLQT1, $K_{ir}2.1$, $K_{ir}2.2$ and KChIP2) currents are substantially less abundant in the human than in the mouse. The lower expression of the ion channels responsible for outward K^+ currents in the human SN explains the expected longer action potential in the SN in the human than in the mouse; a longer action potential in the SN in the human will by itself slow the heart rate. The lower expression of the ion channels responsible for inward currents in the human SN is expected to further slow the heart rate. Finally, the comparison suggests that the expression of SERCA2 in the SN is substantially less abundant in the human than in the mouse and this too may have implications for the heart rate.

Study limitations are considered in the ODS.

Disclosures

None.

Funding Sources

This study was supported by Medtronic Inc.

References

(1) Boyett MR, Honjo H, Kodama I. The sinoatrial node, a heterogeneous pacemaker structure. *Cardiovasc Res* 2000;47:658-687.

(2) DiFrancesco D. Pacemaker mechanisms in cardiac tissue. *Annu Rev Physiol* 1993;55:455-472.

(3) Keith A. The sino-auricular node: a historical note. *Br Heart J* 1942;4:77-79.

(4) Verkerk AO, van Borren MM, Peters RJ, Broekhuis E, Lam KY, Coronel R, de Bakker JM, Tan HL, Wilders R. Single cells isolated from human sinoatrial node: action potentials and numerical reconstruction of pacemaker current. *Conf Proc IEEE Eng Med Biol Soc* 2007;1:904-907.

(5) Tellez JO, Dobrzynski H, Greener ID, Graham GM, Laing E, Honjo H, Hubbard SJ, Boyett MR, Billeter R. Differential expression of ion channel transcripts in atrial muscle and sinoatrial node in rabbit. *Circ Res* 2006;99:1384-1393.

(6) Marionneau C, Couette B, Liu J, Li H, Mangoni ME, Nargeot J, Lei M, Escande D, Demolombe S. Specific pattern of ionic channel gene expression associated with pacemaker activity in the mouse heart. *J Physiol* 2005;562:223-234.

(7) Dobrzynski H, Boyett MR, Anderson RH. New insights into pacemaker activity: promoting understanding of sick sinus syndrome. *Circulation* 2007;115:1921-1932.

(8) Sanchez-Quintana D, Cabrera JA, Farre J, Climent V, Anderson RH, Ho SY. Sinus node revisited in the era of electroanatomical mapping and catheter ablation. *Heart* 2005;91:189-194.

(9) Hoogaars WM, Engel A, Brons JF, Verkerk AO, de Lange FJ, Wong LY, Bakker ML, Clout DE, Wakker V, Barnett P, Ravesloot JH, Moorman AF, Verheijck EE, Christoffels VM. Tbx3 controls the sinoatrial node gene program and imposes pacemaker function on the atria. *Genes Dev* 2007;21:1098-1112.

(10) Maier SKG, Westenbroek RE, Yamanushi TT, Dobrzynski H, Boyett MR, Catterall WA, Scheuer T. An unexpected requirement for brain-type sodium channels for control of heart rate in the mouse sinoatrial node. *Proc Natl Acad Sci USA* 2003;100:3507-3512.

(11) Krapivinsky G, Gordon EA, Wickman K, Velimirovic B, Krapivinsky L, Clapham DE. The G-protein-gated atrial K^+ channel I_{KACh} is a heteromultimer of two inwardly rectifying K^+-channel proteins. *Nature* 1995;374:135-141.

(12) Xu Y, Tuteja D, Zhang Z, Xu D, Zhang Y, Rodriguez J, Nie L, Tuxson HR, Young JN, Glatter KA, Vazquez AE, Yamoah EN, Chiamvimonvat N. Molecular identification and functional roles of a Ca^{2+}-activated K^+ channel in human and mouse hearts. *J Biol Chem* 2003;278:49085-49094.

(13) Lu L, Zhang Q, Timofeyev V, Zhang Z, Young JN, Shin HS, Knowlton AA, Chiamvimonvat N. Molecular coupling of a Ca^{2+}-activated K^+ channel to L-type Ca^{2+} channels via alpha-actinin2. *Circ Res* 2007;100:112-120.

(14) Qu J, Kryukova Y, Potapova IA, Doronin SV, Larsen M, Krishnamurthy G, Cohen IS, Robinson RB. MiRP1 modulates HCN2 channel expression and gating in cardiac myocytes. *J Biol Chem* 2004;279:43497-43502.

(15) Nakamura TY, Pountney DJ, Ozaita A, Nandi S, Ueda S, Rudy B, Coetzee WA. A role for frequenin, a Ca^{2+}-binding protein, as a regulator of K_v4 K^+-currents. *Proc Natl Acad Sci USA* 2001;98:12808-12813.

(16) Bogdanov KY, Vinogradova TM, Lakatta EG. Sinoatrial nodal cell ryanodine receptor and Na^+-Ca^{2+} exchanger : molecular partners in pacemaker regulation. *Circ Res* 2001;88:1254-1258.

(17) Ju Y-K, Chu Y, Chaulet H, Lai D, Gervasio OL, Graham RM, Cannell MB, Allen DG. Store-operated Ca^{2+} influx and expression of TRPC genes in mouse sinoatrial node. *Circ Res* 2007;100:1605-1614.

(18) Courtemanche M, Ramirez RJ, Nattel S. Ionic mechanisms underlying human atrial action potential properties: insights from a mathematical model. *Am J Physiol* 1998;275:H301-H321.

(19) Verkerk AO, Wilders R, van Borren MM, Peters RJ, Broekhuis E, Lam K, Coronel R, de Bakker JM, TanHL. Pacemaker current I_f in the human sinoatrial node. *Eur Heart J* 2007;28:2472-2478.

(20) Lei M, Goddard C, Liu J, Leoni AL, Royer A, Fung SS, Xiao G, Ma A, Zhang H, Charpentier F, Vandenberg JI, Colledge WH, Grace AA, Huang CL. Sinus node dysfunction following targeted disruption of the murine cardiac sodium channel gene Scn5a. *J Physiol* 2005;567:387-400.

(21) Lopez-Santiago LF, Meadows LS, Ernst SJ, Chen C, Malhotra JD, McEwen DP, Speelman A, Noebels JL, Maier SK, Lopatin AN, Isom LL. Sodium channel Scn1b null mice exhibit prolonged QT and RR intervals. *J Mol Cell Cardiol* 2007;43:636-647.

(22) Mangoni E, Couette B, Bourinet E, Platzer J, Reimer D, Striessnig J, Nargeot J. Functional role of L-type $Ca_v1.3$ Ca^{2+} channels in cardiac pacemaker activity. *Proc Natl Acad Sci USA* 2003;100:5543-5548.

(23) Mangoni ME, Traboulsie A, Leoni AL, Couette B, Marger L, Le Quang K, Kupfer E, Cohen-Solal A, Vilar J, Shin HS, Escande D, Charpentier F, Nargeot J. Lory P. Bradycardia and slowing of the atrioventricular conduction in mice lacking $Ca_v3.1$/alpha1G T-type calcium channels. *Circ Res* 2006;98:1422-1430.

(24) Stieber J, Herrmann S, Feil S, Löster J, Feil R, Biel M, Hofmann F, Ludwig A. The hyperpolarization-activated channel HCN4 is required for the generation of pacemaker action potentials in the embryonic heart. *Proc Natl Acad Sci USA* 2003;100:15235-15240.

(25) Miake J, Marban E, Nuss HB. Biological pacemaker created by gene transfer. *Nature* 2002;419:132-133.

(26) Dobrzynski H, Marples DDR, Musa H, Yamanushi TT, Henderson Z, Takagishi Y, Honjo H, Kodama I, Boyett MR. Distribution of the muscarinic K^+ channel proteins $K_{ir}3.1$ and $K_{ir}3.4$ in the ventricle, atrium, and sinoatrial node of heart. *J Histochem Cytochem* 2001;49:1221-1234.

(27) Hagendorff A, Schumacher B, Kirchhoff S, Luderitz B, Willecke K. Conduction disturbances and increased atrial vulnerability in Connexin40-deficient mice analyzed by transesophageal stimulation. *Circulation* 1999;99:1508-1515.

(28) Gaborit N, Le Bouter S, Szuts V, Varro A, Escande D, Nattel S, Demolombe S. Regional and tissue specific transcript signatures of ion channel genes in the non-diseased human heart. *J Physiol* 2007;582:675-693.

(29) Kalman JM, Olgin JE, Karch MR, Hamdan M, Lee RJ, Lesh MD. "Cristal tachycardias": origin of right atrial tachycardias from the crista terminalis identified by intracardiac echocardiography. *J Am Coll Cardiol* 1998;31:451-459.

(30) Pandit SV, Berenfeld O, Anumonwo JM, Zaritski RM, Kneller J, Nattel S, Jalife J. Ionic determinants of functional reentry in a 2-D model of human atrial cells during simulated chronic atrial fibrillation. *Biophys J* 2005;88:3806-3821.

(31) Potapova I, Plotnikov A, Lu Z, Danilo P Jr, Valiunas V, Qu J, Doronin S, Zuckerman J, Shlapakova IN, Gao J, Pan Z, Herron A.J, Robinson RB, Brink PR, Rosen MR, Cohen IS. Human mesenchymal stem cells as a gene delivery system to create cardiac pacemakers. *Circ Res* 2004;94:952-959.

Figure legends

Figure 1. Histological and immunohistochemical characteristics of SN, PN and RA. A, Masson's trichrome stained section through SN. Dashed lines highlight areas sampled for qPCR. B, C, immunolabelling of Cx43 protein at gap junctions (B; green signal) and ANP protein in cytoplasm (C; red signal) in SN, PN and RA. White arrows highlight expressing myocytes; blue arrows highlight non-expressing myocytes.

Figure 2. Relative abundance of mRNA as measured by qPCR for cell type-markers (ANP, Tbx3) and Na^+, Ca^{2+} and HCN channel subunits. Means+SEM (n=6) shown. ^{ab}significantly different from SN (^{a}) or PN (^{b}) (one-way ANOVA); ^{c}significantly different from PN (paired t-test). Individual data for all six subjects are shown by the red points and the outliers are shown by the grey points.

Figure 3. Distribution of ANP, $Na_v1.5$ and $Ca_v1.3$ mRNAs as detected by ISH in SN, PN and RA. A, low power montage of ANP mRNA labelling. Red dotted line highlights SN. B-D, high power images of labelling of ANP, $Na_v1.5$ and $Ca_v1.3$ mRNAs. Labelling of mRNA is in form of dark perinuclear rings. Green arrows highlight ANP expressing myocytes; red arrows highlight ANP non-expressing myocytes.

Figure 4. Expression of $Na_v1.5$ protein in SN, PN and RA. A, high power images of immunolabelling of $Na_v1.5$ protein in cell membrane (red signal) in three tissues. B, high power images of immunolabelling of $Na_v1.5$ protein in cell membrane (red signal) and Cx43 protein at gap junctions (green signal) in three tissues. C, intensity of $Na_v1.5$ protein labelling in SN, PN and RA. Means+SEM (n=4) shown. *†significantly different ($P<0.05$) from SN (*) or PN (†) (one-way ANOVA); ‡ significantly different ($P<0.05$) from PN (paired t-test).

Figure 5. Expression of HCN4 protein in SN, PN and RA. A, low power montage of immunolabelling of HCN4 protein (green signal). White dashed line highlights SN. B, high power images of immunolabelling of HCN4 protein in cell membrane (green signal) in three tissues. Inset shows intensity of HCN4 protein labelling in SN, PN and RA; means+SEM (n=4) shown. *significantly different ($P<0.05$) from SN (one-way ANOVA).

Figure 6. Relative abundance of mRNA as measured by qPCR for K^+ channel subunits. Means+SEM (n=6) shown. ^{ab}significantly different from SN (^{a}) or PN (^{b}) (one-way ANOVA); ^{c}significantly different from PN (paired t-test). Individual data for all six subjects are shown by the red points and the outliers are shown by the grey points.

Figure 7. Relative abundance of mRNA as measured by qPCR for Ca^{2+}-handling proteins, connexins and cell adhesion proteins. Means+SEM (n=6) shown. ^{ab}significantly different from SN (^{a}) or PN (^{b}) (one-way ANOVA); ^{c}significantly different from PN (paired t-test). Individual data for all six subjects are shown by the red points and the outliers are shown by the grey points.

Figure 8. Summary and significance of data. A, B, results of two-way hierarchical cluster analysis (Pearson distances) (A) and multi-dimensional scaling plot (Euclidian distances) (B) of 66 "indicator" mRNAs which had fewer than 2.699 estimated false positive calls in three bootstrap comparisons between SN, PN and RA. In A, red squares indicate values above average for given transcript, white squares average values, and blue squares values below average. These calculations were carried out on normalised $\log_{10}$ expression values. In B, lines separate samples from different tissues. Axes are labelled with arbitrary units. C, human RA action potential as calculated using Courtmanche *et al.*[18] model (left) and human PN and SN action potentials as calculated using modified Courtmanche *et al.*[18] model (middle and right). Membrane potential shown in first row, rate of change of membrane potential (dV/dt) shown in second row and intracellular Ca^{2+} concentration shown in third row. Bottom panel shows base of RA and PN action potentials superimposed. Effect of 'blocking' I_f on SN action potential is shown at top right.

Figure 1

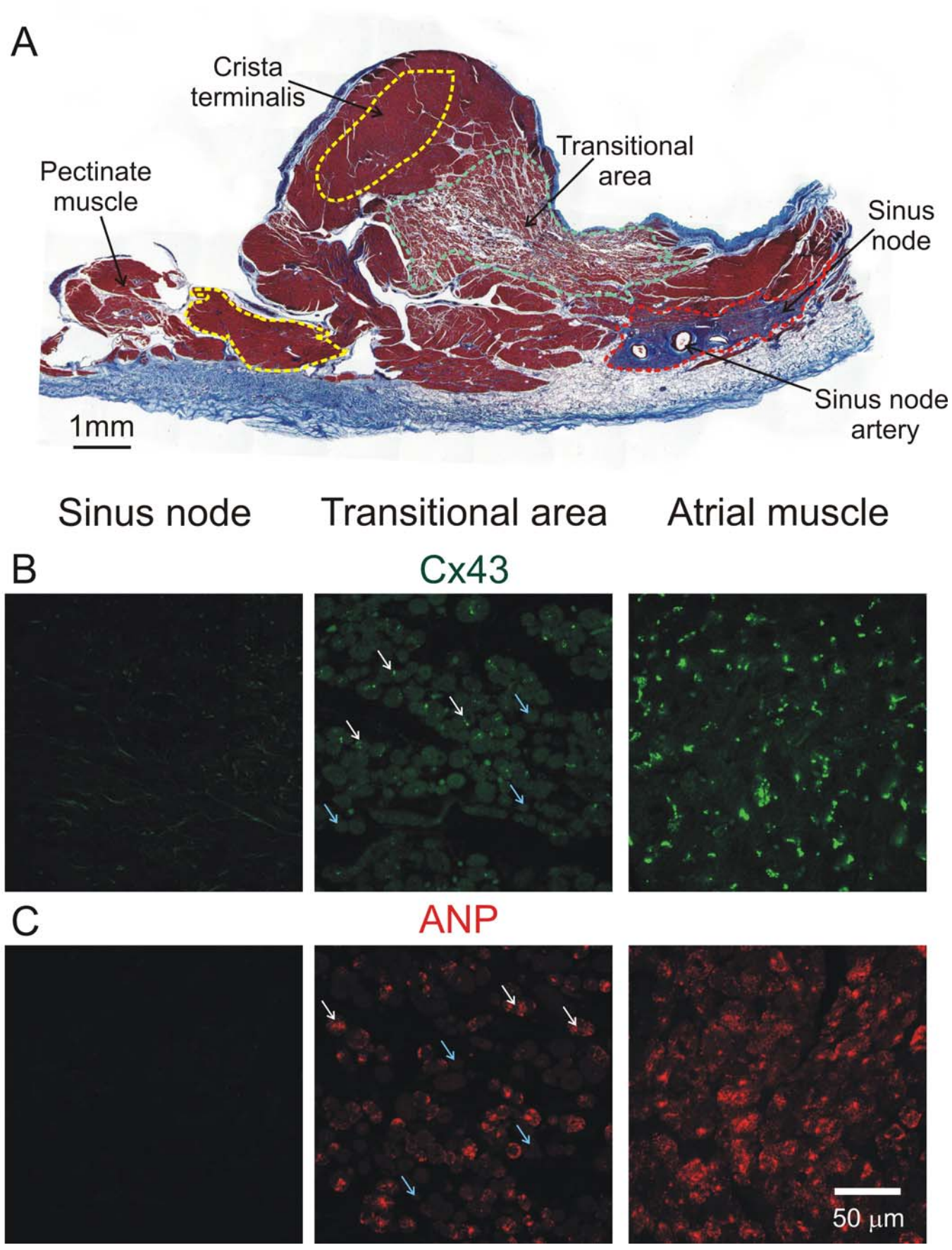
A
Crista terminalis
Transitional area
Pectinate muscle
Sinus node
Sinus node artery
1mm
Sinus node
Transitional area
Atrial muscle
B
Cx43
C
ANP
50 μm

Figure 2

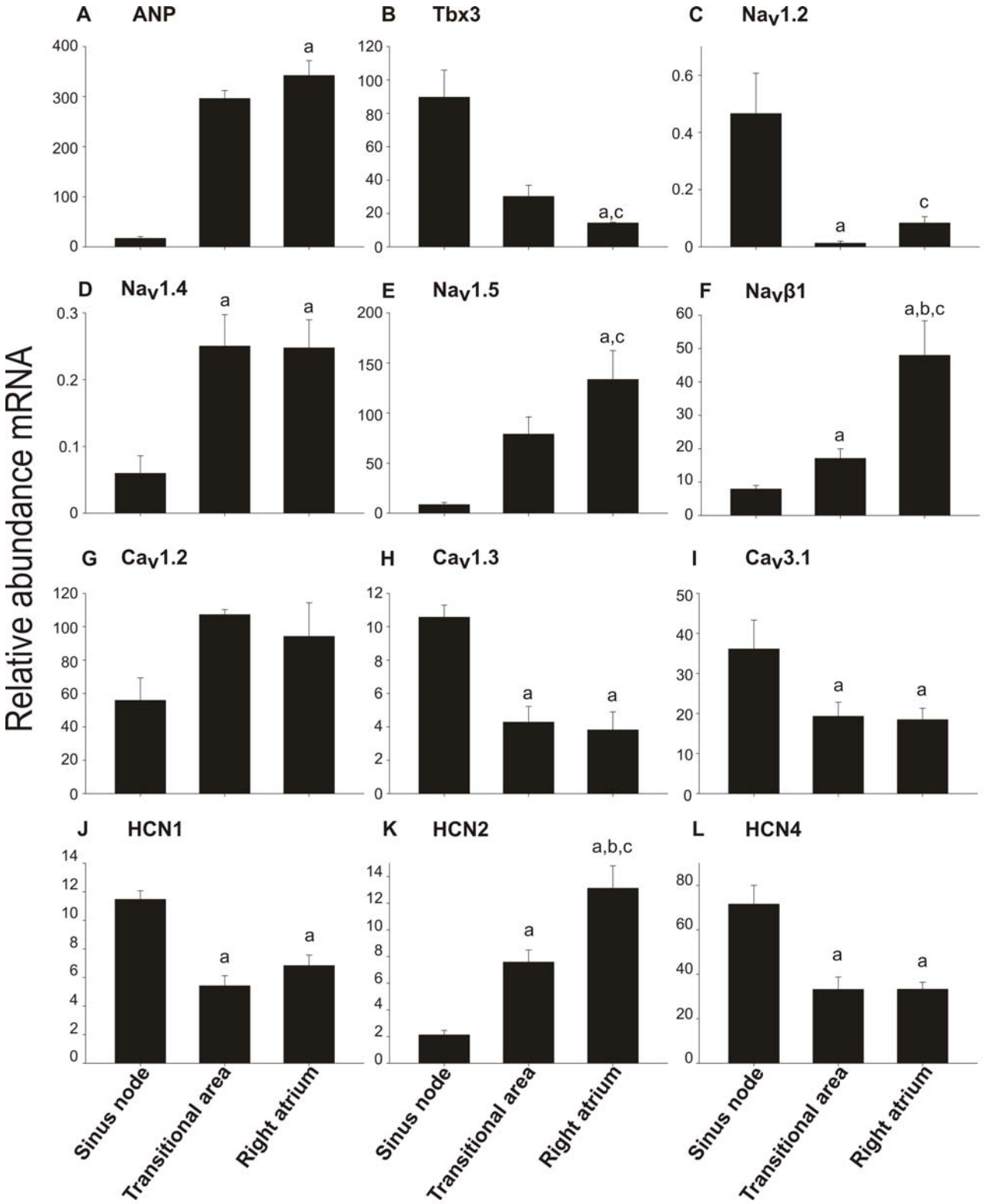
A ANP
B Tbx3
C $Na_V1.2$
D $Na_V1.4$
E $Na_V1.5$
F $Na_V\beta1$
G $Ca_V1.2$
H $Ca_V1.3$
I $Ca_V3.1$
J HCN1
K HCN2
L HCN4
Relative abundance mRNA
Sinus node
Transitional area
Right atrium

Figure 3

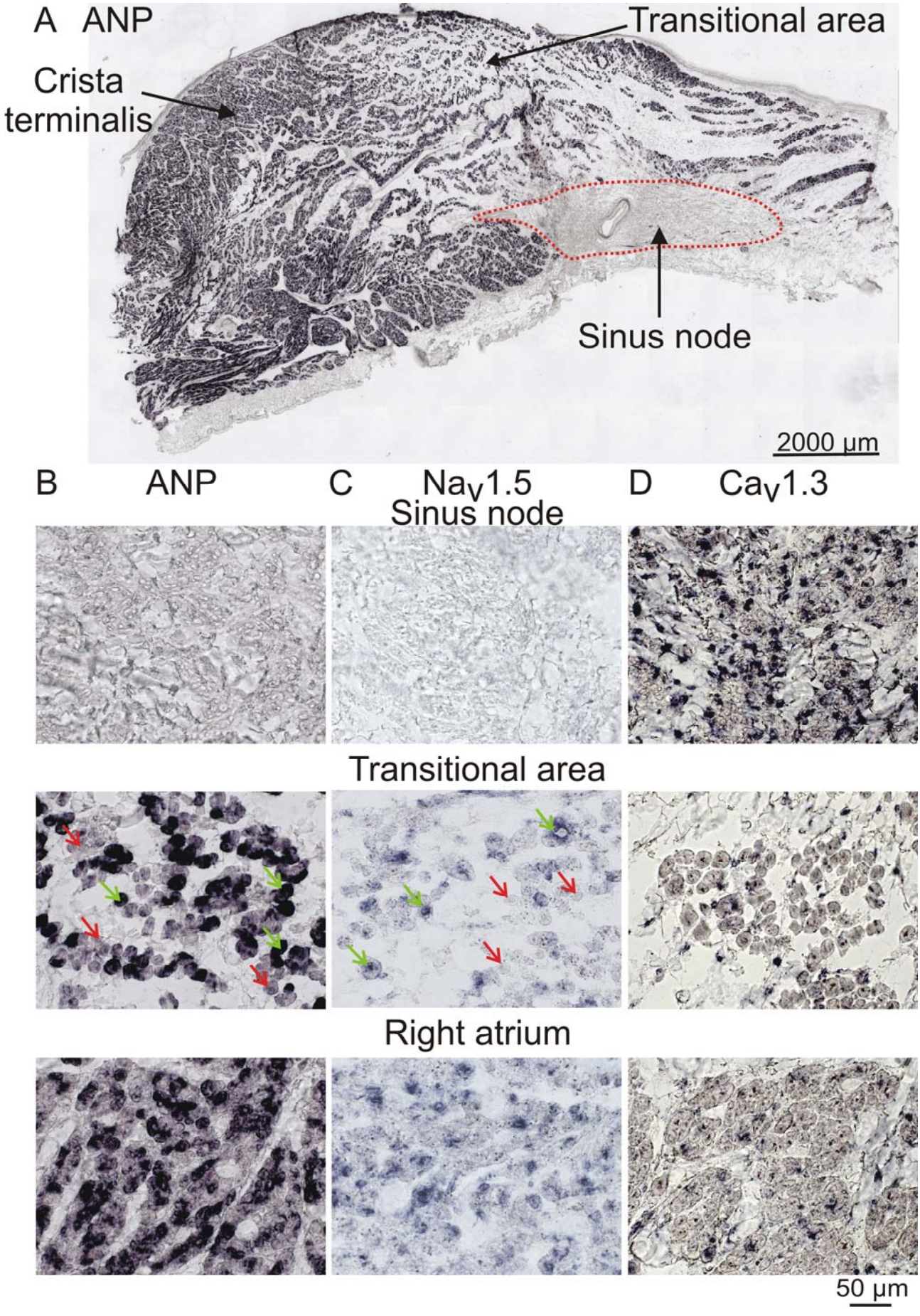
A ANP
Transitional area
Crista terminalis
Sinus node
2000 µm
B ANP
C $Na_V1.5$
D $Ca_V1.3$
Sinus node
Transitional area
Right atrium
50 µm

Figure 4

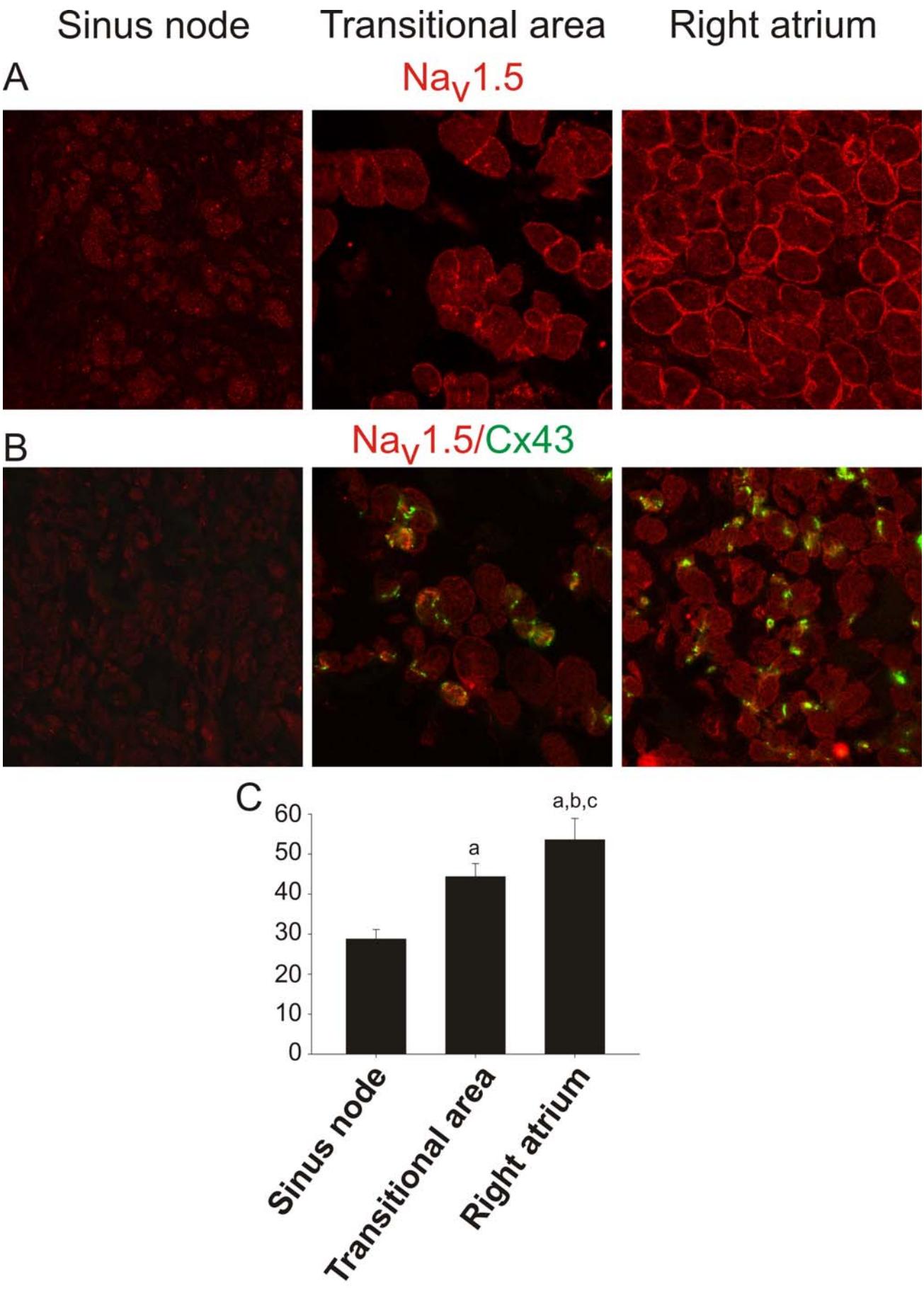
Sinus node
Transitional area
Right atrium
A
$Na_V1.5$
B
$Na_V1.5$/Cx43
C
60
50
40
30
20
10
0
a
a,b,c
Sinus node
Transitional area
Right atrium

Figure 5

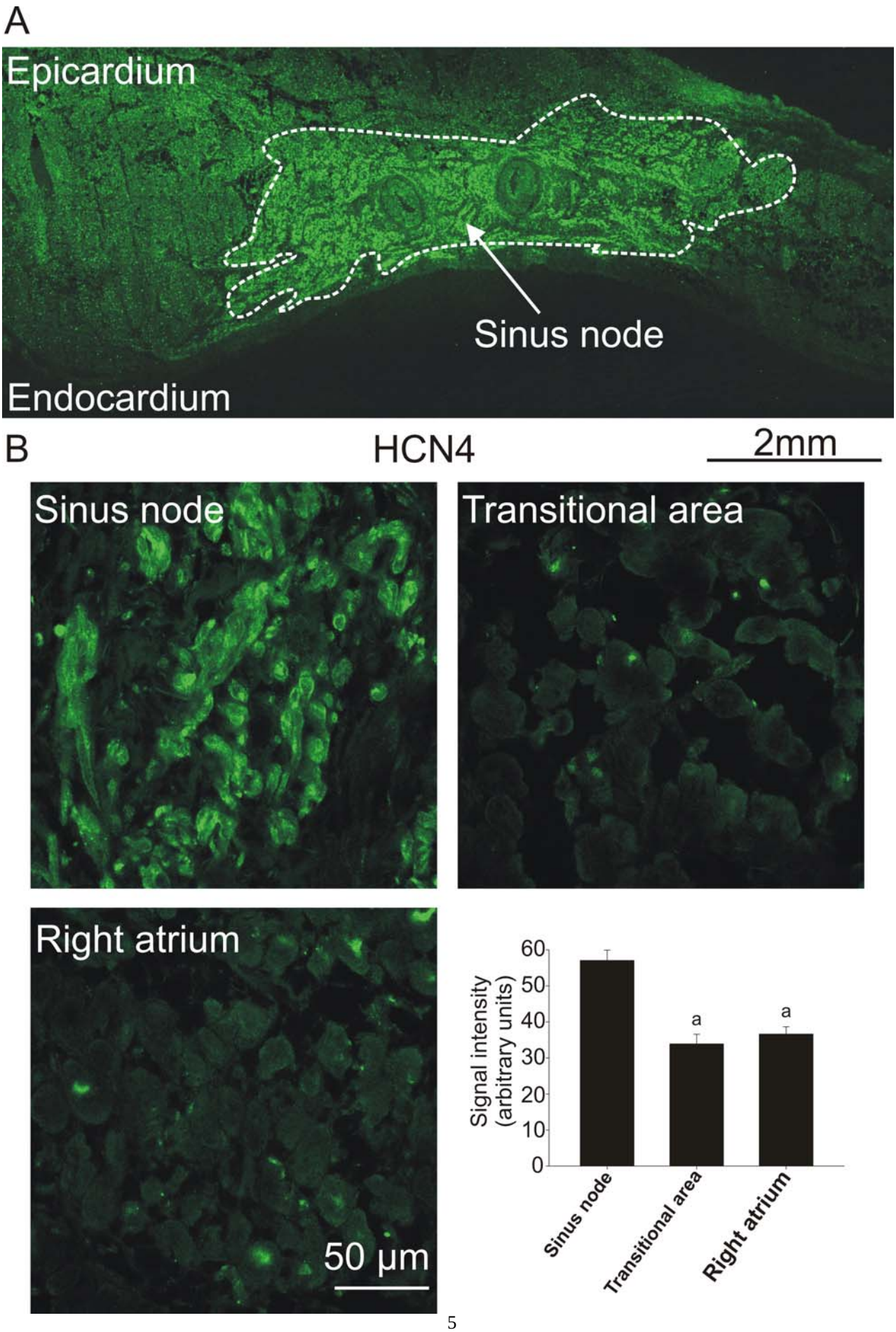
A
Epicardium
Sinus node
Endocardium
B
HCN4
2mm
Sinus node
Transitional area
Right atrium
50 µm
Signal intensity (arbitrary units)
60
50
40
30
20
10
0
a
a
Sinus node
Transitional area
Right atrium

Figure 6

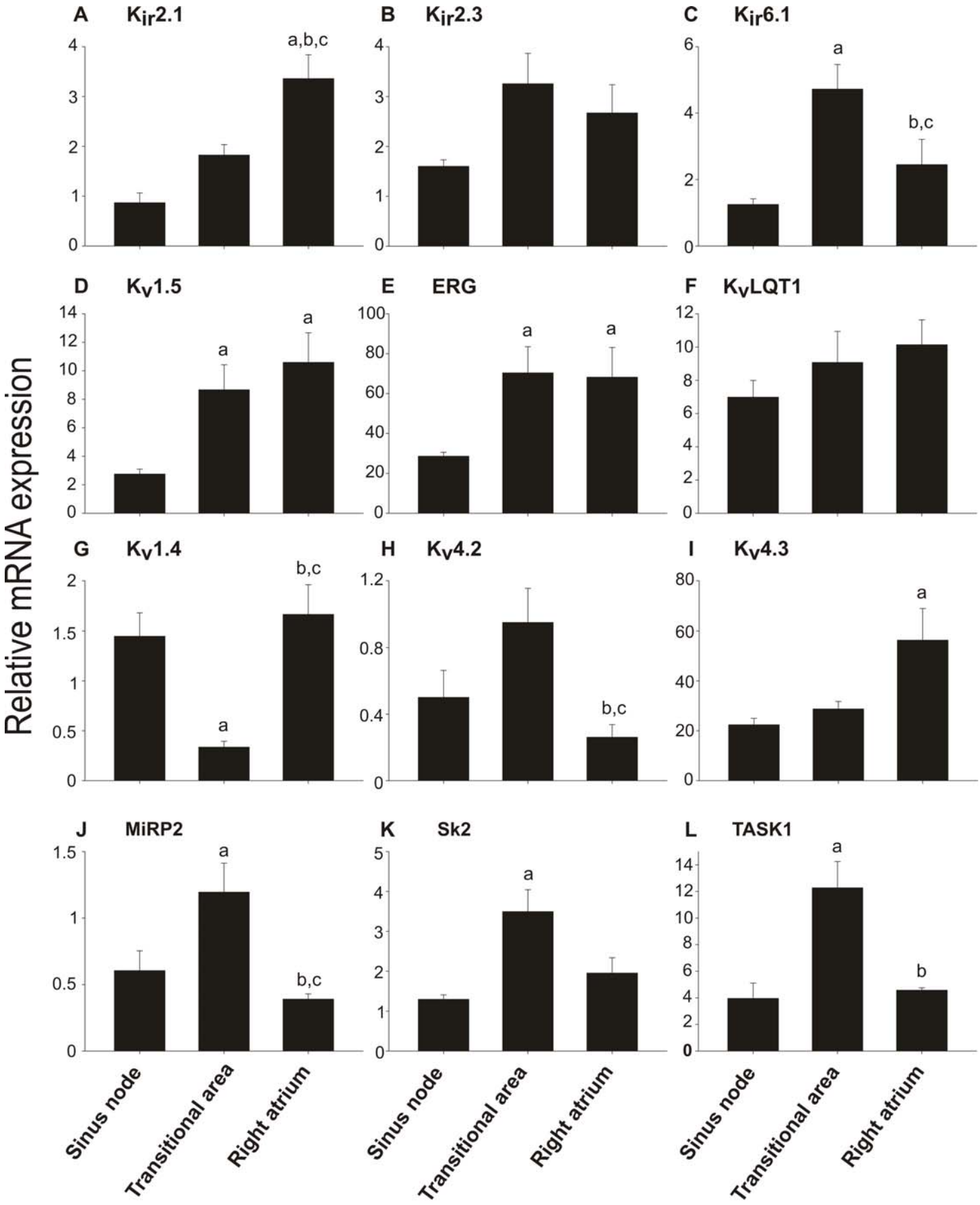
A Kir2.1
a,b,c
B Kir2.3
C Kir6.1
a
b,c
D KV1.5
a
a
E ERG
a
a
F KVLQT1
G KV1.4
b,c
a
H KV4.2
b,c
I KV4.3
a
J MiRP2
a
b,c
K Sk2
a
L TASK1
a
b
Relative mRNA expression
Sinus node
Transitional area
Right atrium

Figure 7

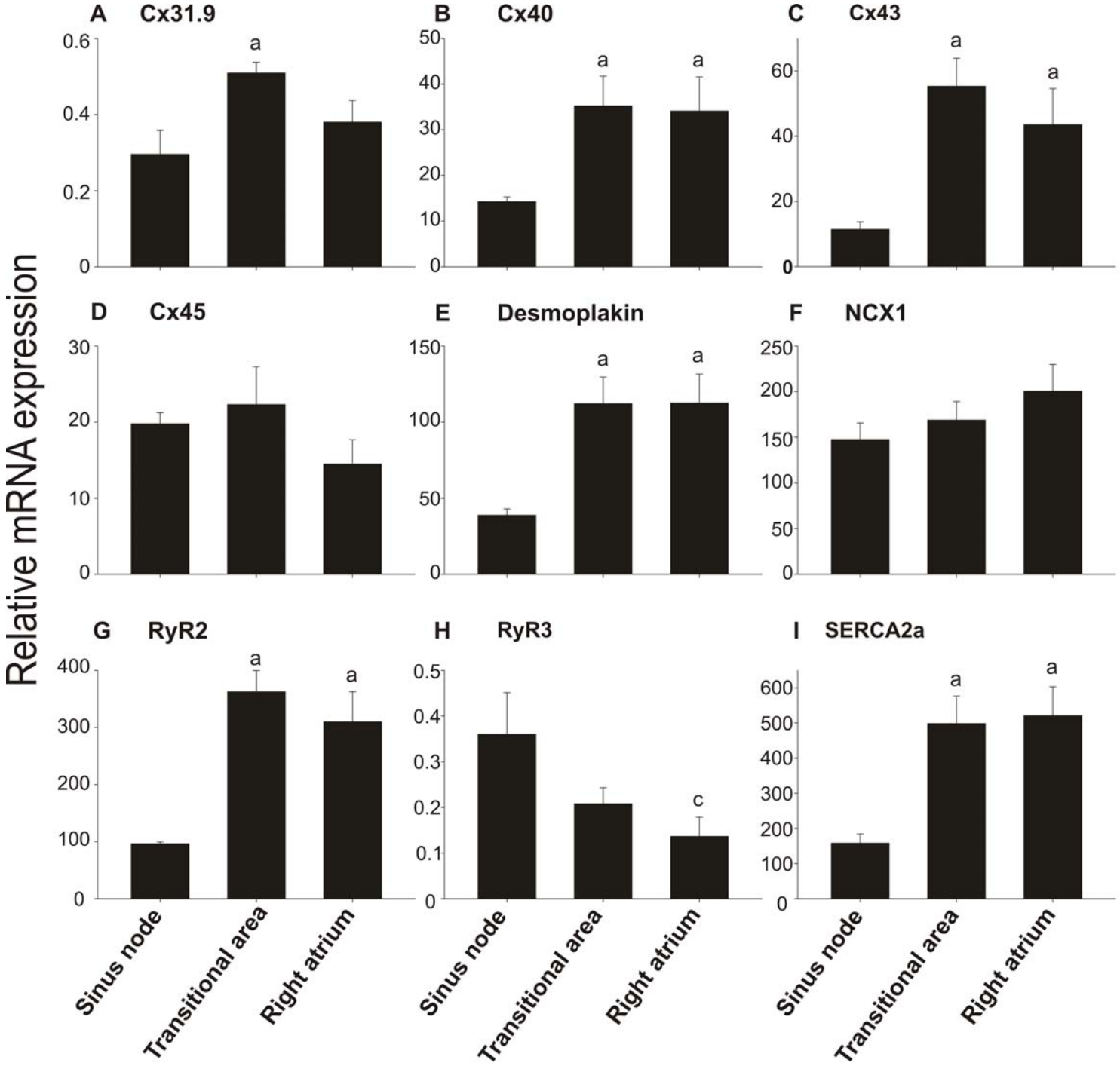
A Cx31.9
B Cx40
C Cx43
D Cx45
E Desmoplakin
F NCX1
G RyR2
H RyR3
I SERCA2a
Relative mRNA expression
Sinus node
Transitional area
Right atrium

Figure 8

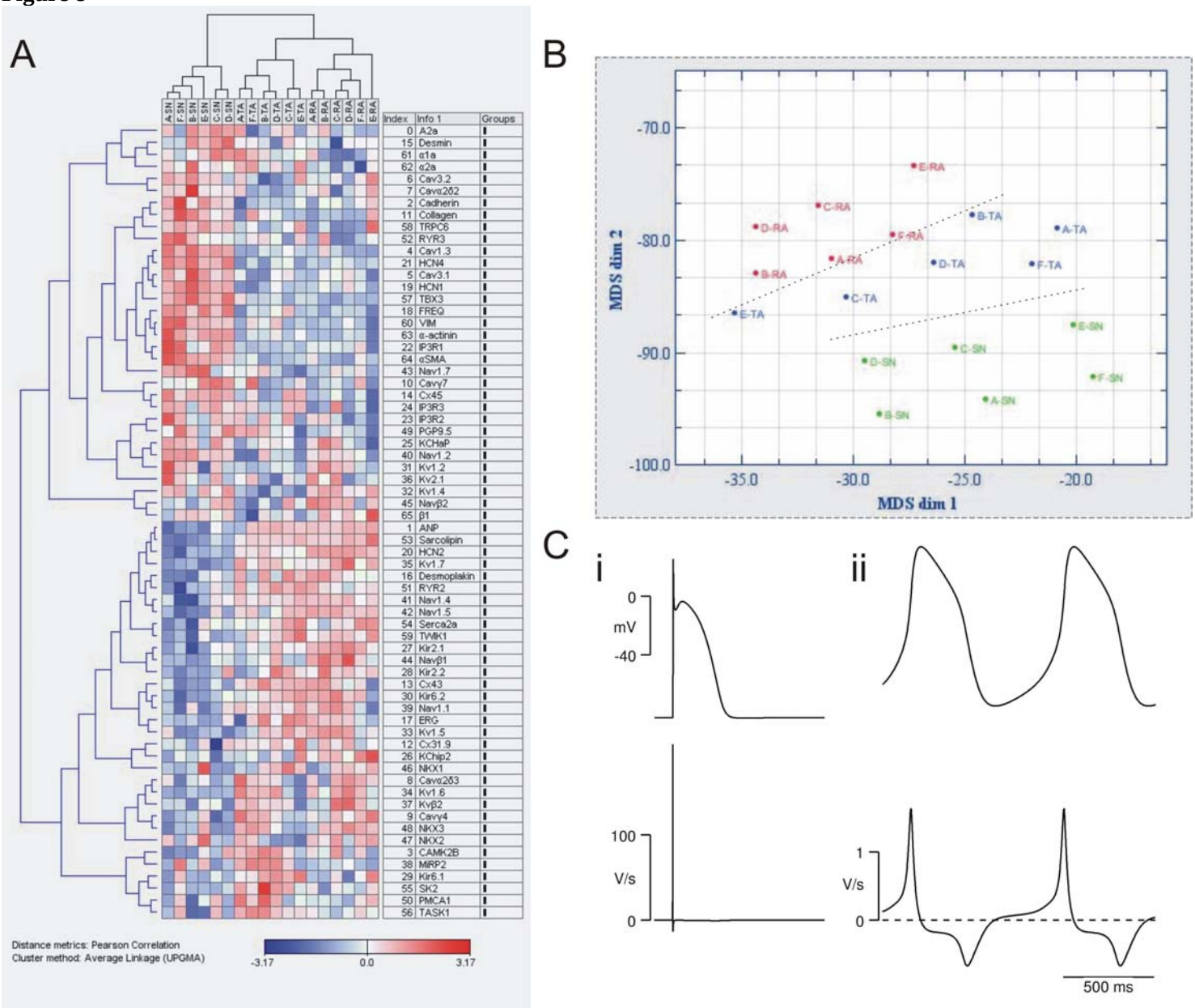
A
A-SN
F-SN
B-SN
E-SN
C-SN
D-SN
A-TA
F-TA
B-TA
D-TA
C-TA
E-TA
A-RA
B-RA
C-RA
D-RA
F-RA
E-RA
Index
Info 1
Groups
0 A2a
15 Desmin
61 α1a
62 α2a
6 Cav3.2
7 Cavα2δ2
2 Cadherin
11 Collagen
58 TRPC6
52 RYR3
4 Cav1.3
21 HCN4
5 Cav3.1
19 HCN1
57 TBX3
18 FREQ
60 VIM
63 α-actinin
22 IP3R1
64 αSMA
43 Nav1.7
10 Cavγ7
14 Cx45
24 IP3R3
23 IP3R2
49 PGP9.5
25 KCHaP
40 Nav1.2
31 Kv1.2
36 Kv2.1
32 Kv1.4
45 Navβ2
65 β1
1 ANP
53 Sarcolipin
20 HCN2
35 Kv1.7
16 Desmoplakin
51 RYR2
41 Nav1.4
42 Nav1.5
54 Serca2a
59 TWIK1
27 Kir2.1
44 Navβ1
28 Kir2.2
13 Cx43
30 Kir6.2
39 Nav1.1
17 ERG
33 Kv1.5
12 Cx31.9
26 KChip2
46 NKX1
8 Cavα2δ3
34 Kv1.6
37 Kvβ2
9 Cavγ4
48 NKX3
47 NKX2
3 CAMK2B
38 MiRP2
29 Kir6.1
55 SK2
50 PMCA1
56 TASK1
Distance metrics: Pearson Correlation
Cluster method: Average Linkage (UPGMA)
-3.17
0.0
3.17
B
-70.0
-80.0
-90.0
-100.0
MDS dim 2
-35.0
-30.0
-25.0
-20.0
MDS dim 1
E-RA
C-RA
D-RA
B-TA
A-TA
F-RA
A-RA
D-TA
F-TA
B-RA
C-TA
E-TA
E-SN
C-SN
D-SN
F-SN
A-SN
B-SN
C
i
ii
0
mV
-40
100
V/s
0
1
V/s
0
500 ms